Nanoscale

Accepted Manuscript

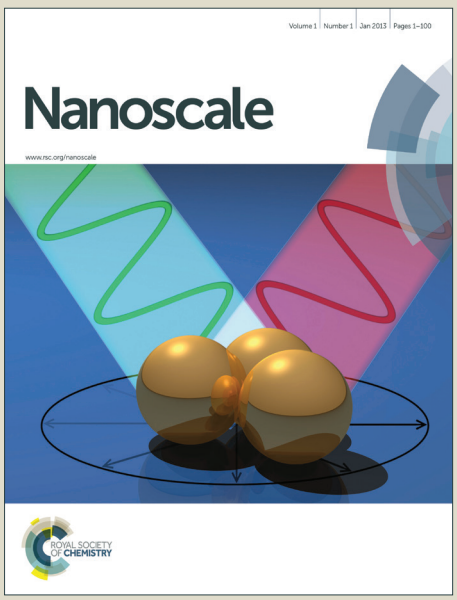

ROYAL SOCIETY OF CHEMISTRY

www.rsc.org/nanoscale

Pumping of water by rotating chiral carbon nanotube

Jia-wei Feng,[a] Hong-ming Ding,[a] Chun-lai Ren[a] and Yu-qiang Ma*[ab]

[a] *National Laboratory of Solid State Microstructures and Department of Physics, Nanjing University, Nanjing 210093, China*

[b] *Center for Soft Condensed Matter Physics and Interdisciplinary Research, Soochow University, Suzhou 215006, China*

∗ *E-mail: myqiang@nju.edu.cn.*

Abstract

Water transportation inside carbon nanotube is of great importance for designing novel nanodevices. In this article, by using molecular dynamics simulations, we systematically investigate the pumping of water by rotating carbon nanotube (CNT). It is found that the chirality and rotation of CNT are two preconditions of stable water flux inside it. Besides, we find that the water flux shows an approximately logarithmic dependence of the angular velocity of the rotation, a linear dependence of the radius of CNT, and interestingly, independence of its length within a certain range of CNT size and angular velocity. Further, we also use a dragging theory which successfully describes the water flux behaviors inside the CNT and can well fit the results obtained from simulations. The present study provides insight into the designing of nanodevices based on the CNT for real applications.

Introduction

Fluid transportation in nanoscale has been attracting great attention[1–3] because of its broad applications in variety of fields such as desalination, energy conversion and drug delivery. Carbon nanotube (CNT) has been intensively studied due to its unique properties since it was found by Iijima in 1991.[4] After 2001, when Hummer and his co-workers found that the water could conduct through the hydrophobic inner space of CNT,[5] more and more attention has been paid to the water behaviors inside the CNT.[6,7] Owing to the frictionless transportation,[7–9] the CNT has become a very promising building block for novel nanofluidic devices.

A deep understanding of pumping of water through CNT is of great importance for their potential applications.[10,11] It is now realized that two conditions, i.e., asymmetry and nonequilibrium, must be satisfied to continuously pump water.[12,13] Hydrostatic pressure is one conventional method to drive water flow.[14] It is also found that osmotic force can be utilized to drive water from the pure water compartment to the salt solution one.[15] Both of the methods above utilize external devices other than CNT. On the contrary, some chemical groups can be decorated to the outside of the CNT. When the CNT is rotating, the chemical groups will drive the water flow like a windmill.[16] Similarly, molecules inside the CNT can also be pumped by a surface wave of CNT.[17] Besides, considering that water has dipole moment, recently, various methods involving electric field or magnetic field to pump water have been proposed.[18–23] Rinne et al.[18] reported the pumping of water by AC electric field, and they attributed the driving force to the Coulomb interaction between the water dipole and the non-uniform electric field. It can also pump water effectively by combing the vibrating charge in the middle part of the CNT and a biased deformation, where the non-equilibrium comes from the charge and the asymmetry from the deformation.[19] Other methods to pump water, such as gradient electric field,[20] rotating electric field with rotating magnetic field,[21] surface energy gradient[24] and thermal gradient,[25] were also reported.

Apart from the methods above, the pumping of water can also be achieved by releasing a pre-twisted CNT.[26] Interestingly, it is also found that when the water flows under hydrostatic pressure, it can in turn induce the rotation of CNT.[27] In this sense, there seems to exist some relation between the water flow and the rotation of the CNT. Inspired by these findings, we propose a new method to pump water which utilizes a rotating chiral CNT. Actually,

the rotation of small molecules (including CNT) can be realized by optical, electrical and chemical means.[28–33] Here, with the help of all-atom molecular dynamics simulations, we systematically investigate the dependence of pumping velocity on the length, radius and angular velocity of the CNT. Moreover, we also use a dragging theory to describe the key features found in our simulations.

Modeling and methods

Molecular dynamics simulations. In this work, we consider a system comprised of one CNT, two graphene sheets and plenty of water molecules (see Fig. 1a). The water molecules are separated into two compartments by the graphene sheets. The atoms of graphene sheets are fixed in all directions, and the central atoms are removed to reserve space for the CNT (see Fig. 1b). Three types of CNT are chosen: one is armchair type with indices (9,9) and length of 3 nm; one is zigzag type with indices (16,0); and another is (n,2n) with length of L, where n varies from 6 to 18 with a step of 2 and L from 3 nm to 10 nm with a step of 1 nm. The radius of the CNT can be simply calculated from its indices (n,m): $R = a/2\pi * \sqrt{n^2 + n * m + m^2}$, where $a = 0.246$ nm. So, in our simulations, the radius ranges from 0.622 nm to 1.865 nm. Further, the CNT is rotating with angular velocity ω, from 0 ps^{-1} to 1.414 ps^{-1}.

All molecular dynamics simulations are performed by using GROMACS 4.6.3 simulation package[34] in the NVT ensemble with the CHARMM36 force field.[35] The temperature is coupled using Nosé-Hoover method[36] at 310 K. TIP3P water model[37] is chosen and the CA type is used for carbon atoms in CNT and graphene. The size of the simulation box depends on the dimensions of the CNT, and the periodic boundary conditions in all directions are always employed. The particle mesh Ewald method[38] is used when calculating the electrostatic interactions, and the Lennard-Jones (LJ) interactions are cut off at a distance of 1.2 nm. The neighbor list is updated every step to avoid the intrinsic errors with low update frequency.[39] The time step is 2 fs, and the data are collected every 2 ps. We conduct 50 ns MD runs for each simulation system, and the last 40 ns of the trajectories are used for further analysis. To ensure the robustness of our results, we also use TIP4P water model[40] with the time step of 1 fs and then compare the results.

Theoretical model. The dragging theory was previously presented by Rinne et al.

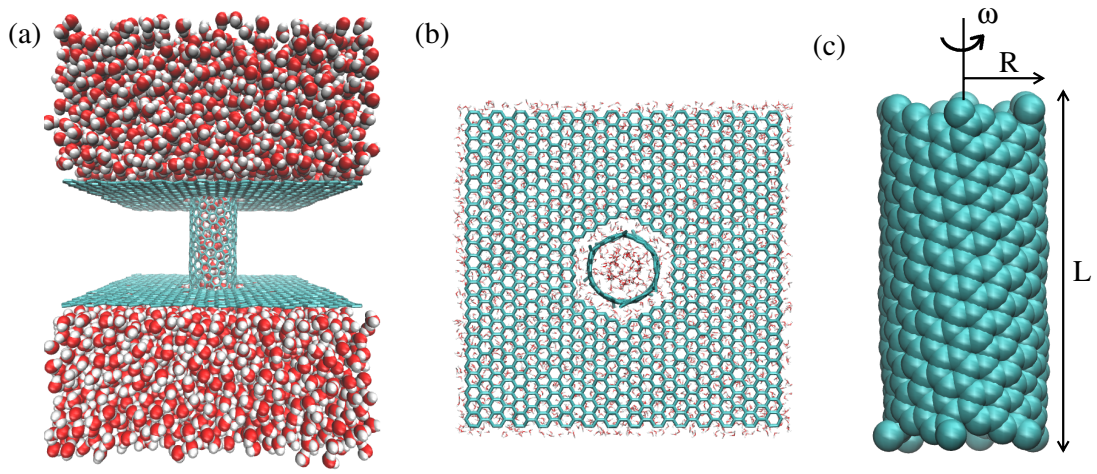

FIG. 1: (a) Snapshot of the simulation system. (b) Top view of the system. Water above the graphene sheets is removed for clarity. (c) The CNT used in our simulations. The length, radius and angular velocity are donated as L, R and ω, respectively.

to calculate the pumping velocity of water under AC electric field.[18] Here, we employ this model to investigate the transportation behaviors of water induced by rotating CNT.

Considering that the raw CNTs are uncharged, there are only LJ interactions between the CNT and the water. On the other hand, as we show in Fig. S1, the water molecules form layered structures inside the CNT (which was also observed in previous report[41]). Therefore, we think that the interaction between CNT and the first layer of water dominates the pumping behaviors since the van der Waals interaction is very short-ranged. Here, to simplify our calculations, we assume that all water molecules in the first layer locate at a certain distance from the wall of the CNT (i.e., the first peak of the radial distribution of water). Further, we find that the correlation length of water inside the CNT is less than 1 nm (see Fig. S2), while the length of the CNT is larger than 3 nm. So, the water can be regarded to be unstructured and distributed continuously, and the density of water molecules obeys the Boltzmann distribution. Thus, the water density profile in equilibrium can be written as

$$\rho_{equ}(\theta, z, \omega, t) = \rho_0 exp(-V(\theta, z, \omega, t)/\epsilon_0), \quad (1)$$

where ρ_0 is the average density of water inside the CNT, ω is the angular velocity of the CNT, $V(\theta, z, \omega, t)$ is the potential between CNT and water at time t, and ϵ_0 is the energy constant

related to the compressibility of water. We should point out that the assumption that water can be regarded to be unstructured and distributed continuously may be invalid in CNTs with smaller diameter, because the correlation length of water inside the CNT will exceed the length of the CNT.[42] Considering the rotation of CNT, we assume a water relaxation time τ which characterizes the time that water spends on responding to the environment. So, the actual water density profile is

$$\rho(\theta, z, \omega, t) = \int_{-\infty}^{t} \frac{1}{\tau} exp((t' - t)/\tau)\rho_{equ}(\theta, z, \omega, t')dt'. \quad (2)$$

The force acting on water along Z direction can be simply deduced by deriving the potential with respect to Z, that is

$$F_z(\theta, z, \omega, t) = -\partial V(\theta, z, \omega, t)/\partial z. \quad (3)$$

And we calculate the total force by integrating the force over θ and z, that is

$$F_{ztol}(\omega, t) = \int_0^{2\pi} \int_0^{L} F_z(\theta, z, \omega, t)\rho(\theta, z, \omega, t)dzd\theta. \quad (4)$$

If the axial velocity of water is constant inside the CNT, we can assume a linear relationship between the total force and the pumping velocity, and we get

$$v_z(\omega, t) = \frac{F_{ztol}(\omega, t)}{\gamma L}. \quad (5)$$

We should notice that the pumping velocity is independent of the time after equilibrium, i.e., $v_z(\omega, t) = v_z(\omega)$. So, the cumulative flux ($Flux_C$), which is defined as the total number of water molecules that have crossed one end of the tube that had previously entered through the other end, should be

$$Flux_C(\omega, t) = Nv_z(\omega)t/L - N, \quad (6)$$

where γ donates the friction coefficient of CNT per unit length and N is the average number of water molecules inside the CNT.

As mentioned above, the last 40 ns of the trajectory is used for analyzing. So the flux rate ($flux_R$), which is defined as the total number of water molecules per nanosecond that have crossed one end of the tube that had previously entered through the other end, will be

$$flux_R(\omega) = \frac{Flux_C(\omega, 50\ ns) - Flux_C(\omega, 10\ ns)}{40\ ns} = \frac{Nv_z(\omega)}{L}. \quad (7)$$

We measure the friction coefficient by applying an additional force to all the water molecules:

$$\gamma = \frac{N * F}{flux_R * L^2}, \tag{8}$$

where all the variables in the right part can be extracted from simulations.

Results and discussion

Potential Energy Landscapes between CNT and Water. As mentioned above, LJ interactions dominate the pumping behaviors and water inside the CNT forms layered structures. Here, in Fig. 2a, we firstly present the potential energy landscape between one water molecule and (6,12) CNT with length of 3 nm at $\theta = 0$ as a function of R and Z. The landscape shows a minimum at $R = 0.29\ nm$ in the range of $1\ nm < Z < 2\ nm$. In line with the potential energy, we also find that the water density profile reaches a maximum at $R = 0.29\ nm$ (see Fig. S1). So, in Fig. 2b, we plot the potential energy landscape as a function of θ and Z at $R = 0.29\ nm$. It is observed that there exists a potential barrier when water escapes from the CNT. While in the middle of the CNT, it shows patterned energy landscape due to the lattice structure of the CNT (the energy difference between the maximum and the minimum is about 0.16 kJ/mol, see Fig. S3). We assume that the pumping velocity is dominated by the energy pattern in the middle part rather than the barrier. It should be noted that the energy difference seems to be rather small compared with the thermal fluctuation. However, owing to the low friction of the CNT, applying a small force will result in a large water flux.[7–9] Further, to investigate the pumping behaviors, we need a general expression to describe the energy landscape (as far as we know, there is no previous report). Here, we propose an empirical expression that well interpolates the energy landscapes (see Fig. S3 and S4), which is written as

$$\begin{aligned} V(\theta, z, \omega, t) =& asin(n(\frac{5}{\sqrt{3}r}z + \theta - \omega t)) + bcos(n(\frac{5}{\sqrt{3}r}z + \theta - \omega t)) + \\ & csin(2n(\frac{2}{\sqrt{3}r}z - \theta + \omega t)) + dcos(2n(\frac{2}{\sqrt{3}r}z - \theta + \omega t)) + \\ & esin(3n(\frac{1}{3\sqrt{3}r}z + \theta - \omega t)) + fcos(3n(\frac{1}{3\sqrt{3}r}z + \theta - \omega t)) + V_0, \end{aligned} \tag{9}$$

where r donates the radius of the CNT, and a, b, c, d, e, f and V_0 are fitted from the energy landscape.

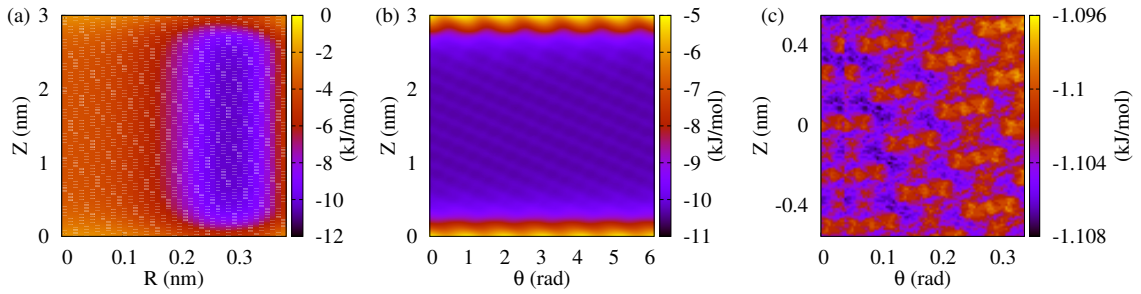

FIG. 2: (a) Potential energy landscape as a function of R and Z at $\theta = 0$ (b) Potential energy landscape as a function of θ and Z at $R = 0.29\ nm$. (c) Potential energy landscape of (18,36) CNT as a function of θ and Z at $r = 1.29\ nm$.

To illustrate the interactions between the CNT and different layers of water, in Fig. 2c, we show the potential energy landscapes of (18,36) CNT at $r = 1.29\ nm$ (the second peak of the water density profile). It is found that the potential energy landscape is greatly smoothed as compared with that at the first peak of the water density profile (see Fig. S3), and since the pumping force comes from the derivation of the potential, we believe it is a reasonable assumption that the interaction between the CNT and the first layer of water dominates the pumping behaviors.

Pumping Behaviors of Water inside CNTs. By using molecular dynamics simulations, we firstly investigate the water flux inside an armchair (9,9) CNT and a zigzag (16,0) CNT (without chirality). As shown in Fig. 3a, we find that the CNTs cannot pump water under any of the angular velocities (very little cumulative flux may be due to thermal fluctuations). This is because the CNT is intrinsically symmetric, and although the CNT is forced to rotate, it can not induce the unidirectional water flow. Similar phenomenon is observed in (6,12) CNT with zero angular velocity. Despite the asymmetry, the system is in equilibrium. Thus the system will also generate zero water flux. Our observations confirm that the two conditions (i.e., asymmetry and nonequilibrium) are truly required to continuously pump water.

We then explore the relationship between water flux inside a (6,12) CNT and angular velocity as well as the length of CNT. The friction coefficient of the CNT is measured as $3.03 * 10^{-4}\ kg * m^{-1} * s^{-1}$ (see Fig. S5). Then the parameters in dragging theory are fitted to

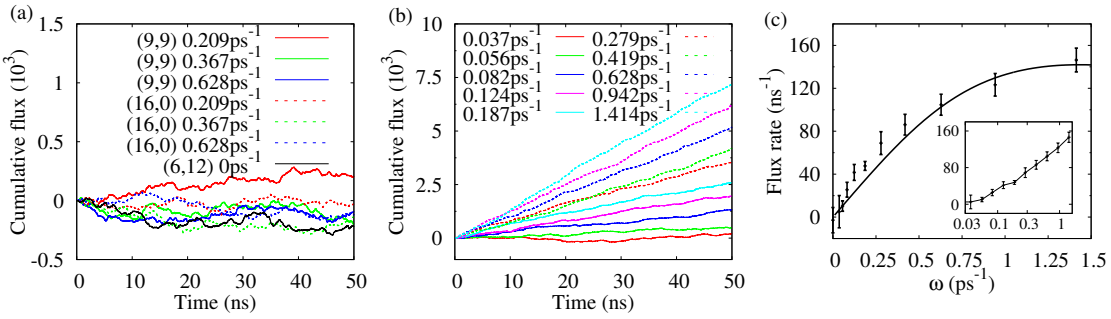

FIG. 3: (a) Cumulative flux inside (9,9) and (16,0) CNTs with different angular velocities and a frozen (6,12) CNT. (b) Cumulative flux inside (6,12) CNT with length of 3 nm as a function of time for different angular velocities. (c) Flux rate inside (6,12) CNT with length of 3 nm as a function of angular velocity. the simulation results (data points) are compared with dragging theory (line). The inset shows the simulation results in logarithmic scale.

the simulation results (see Fig. 3b, c), and we can get $\tau = 0.12\ ps$, $\epsilon_0 = 0.17\ kJ$. We observe that the water flux rate shows approximately logarithmic dependence of the angular velocity (see the inset in Fig. 3c), and the theoretical predictions are in good agreement with the simulation results. In particular, when the CNT is fixed, namely the angular velocity is zero, there will exist no water flux. And the water flux increases with the angular velocity in the range of 0 ps^{-1} to 0.6 ps^{-1}. However, the pumping becomes inefficient when we continue to increase the angular velocity because the oscillation period of the potential energy is close to the relaxation time of water, and water molecules inside the CNT are unable to adjust its position to the quickly changing environment. Such tendency has also been observed in the angular velocity of water (see Fig. S6). By carefully analyzing the trajectories, we find that the average density of water inside the CNT doesn't change under different angular velocities, inferring that the increment of the flux is a result of the increment of pumping velocity under larger angular velocity. We should point out that the theory also predicts the water flux will decrease under angular velocity larger than 1.5 ps^{-1} (the predicted flux decreases to 40 ns^{-1} in the case of 10 ps^{-1}, and it is zero under infinite angular velocity). However, the simulation package crashes under higher angular velocity, and actually the high angular velocity of carbon atom is also very hard to realize experimentally.[32] To show the robustness of our findings, we also do extra simulations with different water model and different time steps as mentioned in the methods section. As shown in Fig. S7, although

there exist some slight deviations between the results, the water flux shows the same trend. This indicates that our results are nearly independent of water model and time step, and we will use only the TIP3P water model and time step of 2 fs in our following simulations.

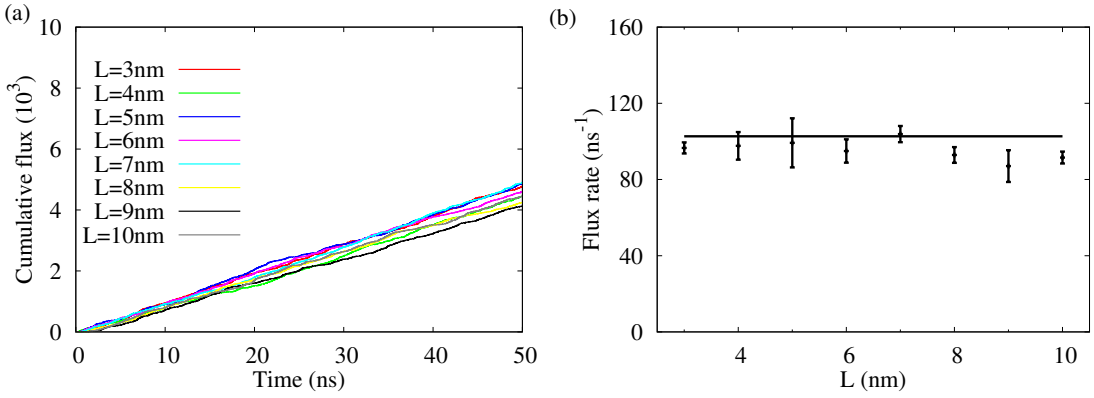

FIG. 4: (a) Cumulative flux inside (6,12) CNT with angular velocity of 0.628 ps^{-1} as a function of time for different lengths. (b) Flux rate inside (6,12) CNT with angular velocity of 0.628 ps^{-1} as a function of length. The simulation results (data points) are compared with dragging theory (line).

We then investigate the effect of CNT length on the water flux. As shown in Fig. 4, the flux is nearly independent of the length of CNT. This can be explained by imaging a new system which comprises two identical CNTs with length of 3 nm and the CNTs are connected end-to-end. The system is apparently equivalent to another system that comprises one single CNT with length of 6 nm. However, since the water velocities inside the two CNTs are both equal to that inside a 3 nm CNT, the system will generate the same water flux. Our observation is also in line with the prediction of the dragging theory: With the increase of the length, it will increase both the pumping force and the total friction, therefore it won't affect the pumping velocity (which is equal to the ratio of force to friction). Besides, it is also observed that the prediction is little deviated from the simulation results, which may be arisen from the ignoring of the energy barrier at the entrance of the CNT.

Next, we show the flux rate inside CNTs with different radius for $L = 10$ nm and $\omega R = 0.389$ nm/ps (equal to the velocity of carbon atoms in a (6,12) CNT with angular velocity of 0.628 ps^{-1}). As shown in Fig. 5, the flux rate increases linearly with the radius. Notice that the pumping force comes from the interaction between the first layer of water

and the wall of the CNT, and the circumference of the wall is directly proportional to the radius. It is therefore reasonable to expect the linear relationship. However, it is hard to get a general expression between the flux rate and the radius since the potential landscapes are very different (see Fig. S3), and the effective parameters (i.e., the friction coefficient, the compressibility of water and the relaxation time) change with the indices of the CNT. As illustrated in Fig. S8, by fitting the simulation results using (14,28) CNT, we get $\gamma = 7.30 * 10^{-4}\ kg * s^{-1} * m^{-1}$, $\tau = 0.40\ ps$ and $\epsilon_0 = 0.74\ kJ$. By comparing with those in the case of (6,12) CNT ($\gamma = 3.03 * 10^{-4}\ kg * s^{-1} * m^{-1}$, $\tau = 0.12\ ps$, $\epsilon_0 = 0.17\ kJ$), we find that the parameters are actually effective ones and will be changed in different confined environments. It should be noted that the linear relationship is based on the assumption that the axial velocities of water molecules are constant inside the CNT. And we find they are indeed the same in our simulations (see Fig. S9). However, the inner water and the first layer of water may have different axial velocities with the increase of the diameter or the decrease of the length of CNT. Actually, we have seen this tendency in (18,36) CNT with diameter of 3.7 nm and length of 10 nm. So the linear relationship is only valid if the length of the CNT is much larger than the radius.

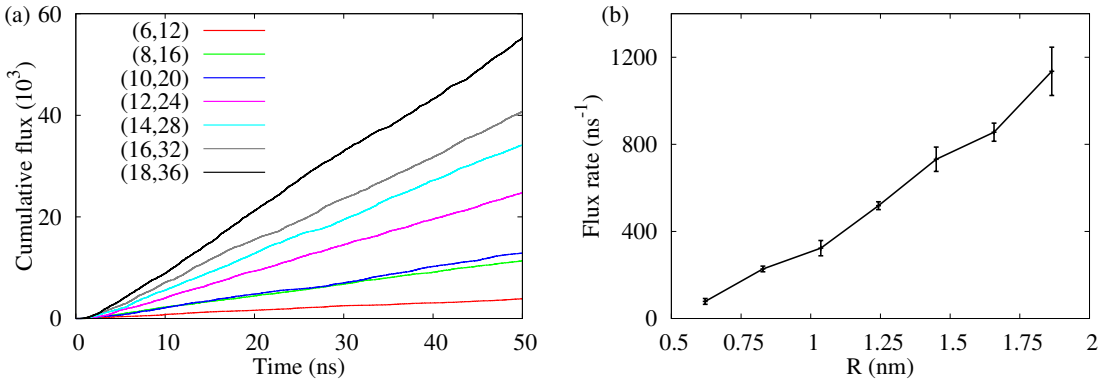

FIG. 5: (a) Cumulative flux inside CNTs with length of 10 nm as a function of time for different radius. (b) Flux rate inside CNTs as a function of the radius of the CNT. The points are connected to guide the eye.

Finally, based on the above result(the pumping behaviors are dominated by the potential energy landscape and the angular velocity), we try to enhance the pumping efficiency by increasing the interaction strength between the water and the CNT (which will increase

the difference between the maximum and the minimum of the potential energy landscape). Here we decorate the CNT with partial charge from +0.05e to +0.4e (see Fig. S10), which enhances the electrostatic interaction. All together, 140 carbon atoms are modified and the total charge is from +7e to +56e. As shown in Fig. 6, we find that the modified CNTs with partial charge +0.05e to +0.2e successfully show larger flux rate. By carefully analyzing the result, we find that the enhancement is comprised of two parts, i.e., the larger average density of water inside the CNT and the larger pumping velocity, which are both induced by the enhanced interaction between water and the CNT. The results further confirm the validity of the dragging theory. However, continuing to increase the interaction between CNT and water will result in a smaller water flux, and the water flux is almost zero when the CNT is decorated with partial charge +0.4e. In this case, the interaction is so high that water cannot diffuse freely, which has already been observed in previous studies.[43,44] Following the above result, we also design a functionalized CNT by bonding hydrogen atoms to the surface of the CNT (see Fig. S11). The carbon atoms are partially charged after the functionalization (the force field parameters are taken from previous work[45]), which will also increase the interaction between water and the CNT moderately. As shown in Fig. 6, the functionalized CNT truly shows enhanced pumping velocity.

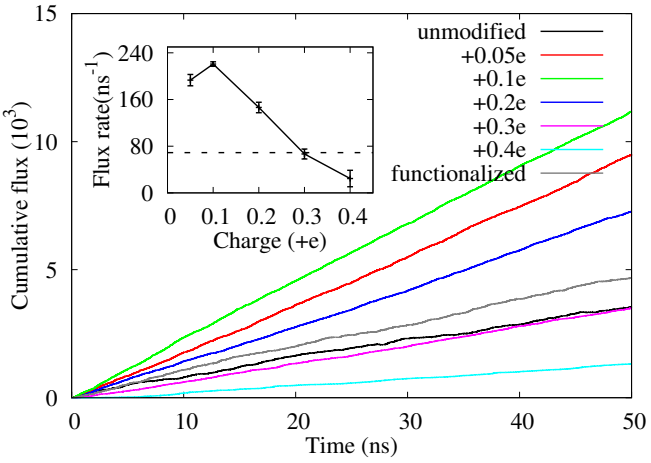

FIG. 6: Cumulative flux inside a raw and decorated CNTs as a function of time. The inset shows the flux rate inside CNTs as a function of partial charge. The dashed line indicates the average flux rate inside a raw CNT.

Conclusions

In summary, here we propose a novel method to pump water by the rotation of chiral CNT without external devices. We find that the water flux increases logarithmically with the angular velocity, linearly with the radius of the CNT. And interestingly, it shows no dependence of the length of the CNT, which may be helpful in designing ultra-short nanodevices without the expense of pumping velocity. The relationship is valid under conditions that the angular velocity of the CNT is not too large (i.e., less than 1.4 ps^{-1}), the length of the CNT is larger than the correlation length of water inside the CNT, and the axial velocity of water inside the CNT is nearly the same. Most of the CNTs produced in experiment have the diameter of about several nanometers, and the length longer than 100 nm, which satisfy these conditions according to our previous discussions. Importantly, we also employ a dragging theory which can well describe most of the findings in our simulations. Under the guidance of the theory, we successfully design a functionalized CNT with higher pumping efficiency. Experimentally, the ultra-short CNT can be embedded into a lipid membrane acting like a biological water channel.[46] In addition, previous report also showed that a much longer CNT could embed into a silicon nitride membrane,[47] where the membrane is used to separate two water compartments and only allows water to pass through the inner space of the CNT. Since CNTs in these structures are not covalently bonded to the surrounding membrane, they can be rotated if a torque is applied (e.g., using the optical tweezers[33]). Since the driving force (i.e., van der Waals interaction and electrostatic interaction in some cases) exists between the CNT and all kinds of materials, the mechanism can be used to pumping other materials such as gases and drugs. Thus, our findings may provide useful guidelines in designing novel CNT based nanodevices.

Acknowledgments: This work is supported by the National Natural Science Foundation of China (No. 91027040), and the National Basic Research Program of China (No. 2012CB821500). We are grateful to the High Performance Computing Center (HPCC) of Nanjing University for doing the numerical calculations in this paper on its IBM Blade cluster system.

[1] W. Sparreboom, A. van den Berg and J. C. T. Eijkel, *New J. Phys.,* 2010, **12,** 015004.

[2] J. Y. Su and H. X. Guo, *J. Phys. Chem. B,* 2013, **117,** 11772-11779.

[3] J. Bai and X. C. Zeng, *Proc. Natl. Acad. Sci. U.S.A.,* 2012, **109,** 21240-21245.

[4] S. Iijima, *Nature,* 1991, **354,** 56-58.

[5] G. Hummer, J. C. Rasaiah and J. P. Noworyta, *Nature* 2001, **414,** 188-190.

[6] D. J. Bonthuis, K. F. Rinne, K. Falk, C. Nadir Kaplan, D. Horinek, A. Nihat Berker, L. Bocquet and R. R. Netz, *J. Phys.: Condens. Matter,* 2011, **23,** 184110.

[7] M. Whitby and N. Quirke, *Nat. Nanotechnol.,* 2007, **2,** 87-94.

[8] M. Majumder, N. Chopra, R. Andrews, and B. J. Hinds, *Nature,* 2005, **438,** 44.

[9] J. K. Holt, H. G. Park, Y. Wang, M. Stadermann, A. B. Artyukhin, C. P. Grigoropoulus, A. Noy and O. Bakajin, *Science,* 2006, **312,** 1034-1037.

[10] B. Liu, X. Y. Li, B. L. Li, B. Q. Xu and Y. L. Zhao, *Nano Lett.,* 2009, **9,** 1386-1394.

[11] J. Y. Li, X. J. Gong, H. J. Lu, D. Li, H. P. Fang and R. H. Zhou, *Proc. Natl. Acad. Sci. U.S.A.,* 2007, **104,** 3687-3692.

[12] R. D. Astumian, *Science,* 1997, **276,** 917.

[13] P. Král and B. Y. Wang, *Chem. Rev.,* 2013, **113,** 3372-3390.

[14] M. Whitby, L. Cagnon, M. Thanou and N. Quirke, *Nano Lett.,* 2008, **8,** 2632-2637.

[15] A. Kalra, S. Garde and G. Hummer, *Proc. Natl. Acad. Sci. U.S.A.,* 2003, **100,** 10175-10180.

[16] B. Y. Wang and P. Král, *Phys. Rev. Lett.,* 2007, **98,** 266102.

[17] Z. Insepov, D. Wolf and A. Hassanein, *Nano Lett.,* 2006, **6,** 1893-1895.

[18] K. F. Rinne, S. Gekle, D. J. Bonthuis and R. R. Netz, *Nano Lett.,* 2012, **12,** 1780-1783.

[19] X. Y. Zhou, F. M. Wu, J. L. Kou, X. C. Nie, Y. Liu and H. J. Lu, *J. Phys. Chem. B,* 2013, **117,** 11681-11686.

[20] Y. Wang, Y. J. Zhao and J. P. Huang, *J. Phys. Chem. B,* 2011, **115,** 13275-13279.

[21] X. P. Li, G. P. Kong, X. Zhang and G. W. He, *Appl. Phys. Lett.,* 2013, **103,** 143117.

[22] J. Y. Su and H. X. Guo, *ACS Nano,* 2011, **5,** 351-359.

[23] X. J. Gong, J. Y. Li, H. J. Lu, R. Z. Wan, J. C. Li, J. Hu, and H. P. Fang, *Nat. Nanotechnol.,* 2007, **2,** 709-712.

[24] J. L. Kou, M. F. Mei, H. J. Lu, F. M. Wu and J. T. Fan, *Phys. Rev. E,* 2012, **85,** 056301.

[25] H. A. Zambrano, J. H. Walther, P. Koumoutsakos and I. F. Sbalzarini, *Nano Lett.,* 2009, **9,** 66-71.

[26] W. H. Duan and Q. Wang, *ACS Nano,* 2010, **4,** 2338-2344.

[27] L. N. Zhao, Y. L. Zhao and R. H. Zhou, *J. Phys. Chem. C,* 2012, **116,** 13429-13434.

[28] T. R. Kelly, H. De Silva and R. A. Silva, *Nature,* 1999, **401,** 150-152.

[29] N. Koumura, R. W. Zijlstra, R. A. van Delden, N. Harada and B. L. Feringa, *Nature* 1991, **401,** 152-155.

[30] P. Král and H. Sadeghpour, *Phys. Rev. B,* 2002, **65,** 161401.

[31] P. Král and T. Seideman, *J. Chem. Phys.,* 2005, **123,** 184702.

[32] A. Lehmuskero, R. Ogier, T. Gschneidtner, P. Johansson and M. Käll, *Nano Lett.* 2013, **13,** 3129-3134.

[33] J. L. Zhang, T. G. Kim, S. C. Jeoung, F. F. Yao, H. W. Lee and X. D. Sun, *Opt. Commun.,* 2006, **267,** 260-263.

[34] B. Hess, C. Kutzner, D. Van Der Spoel and E. Lindahl, *J. Chem. Theory Comp.,* 2008, **4,** 435-447.

[35] P. Bjelkmar, P. Larsson, M. A. Cuendet, B. Hess and E. Lindahl, *J. Chem. Theory Comput.,* 2010, **6,** 459-466.

[36] S. Nosé, *J. Chem. Phys.,* 1984, **81,** 551-519.

[37] W. L. Jorgensen, J. Chandrasekhar, J. D. Madura, R. W. Impey and M. L. Klein, *J. Chem. Phys.,* 1983, **79,** 926-935.

[38] U. Essmann, L. Perera, M. L. Berkowitz, T. Darden, H. Lee and L. G. Pedersen, *J. Chem. Phys.,* 1995, **103,** 8577-8593.

[39] J. Wong-ekkabut, M. S. Miettinen, C. Dias and M. Karttunen, *Nat. Nanotechnol.,* 2010, **5,** 555-557.

[40] J. L. F. Abascal and C. Vega, *J. Chem. Phys.,* 2005, **123,** 234505.

[41] S. Joseph and N. R. Aluru, *Nano Lett.,* 2008, **8,** 452-458.

[42] J. Thomas, and A. McGaughey, *Phys. Rev. Lett.,* 2009, **102,** 184502.

[43] X. J. Gong, J. Y. Li, H. Zhang, R. Z. Wan, H. J. Lu, S. Wang and H. P. Fang, *Phys. Rev. Lett.,* 2008, **101,** 257801.

[44] Y. L. Yang, X. Y. Li, J. L. Jiang, H. L. Du, L. N. Zhao and Y. L. Zhao, *ACS Nano,* 2010, **4,** 5755-5762.

[45] D. A. Mooney, F. Müller-Plathe and K. Kremer, *Chem. Phys. Lett.,* 1998, **294,** 135-142.

[46] L. Liu, C. Yang, K. Zhao, J. Y. Li and H. C. Wu, *Nat. Commun.,* 2013, **4,** 2989.

[47] J. K. Holt, A. Noy, T. Huser, D. Eaglesham and O. Bakajin, *Nano Lett.,* 2004, **4,** 2245-2250.

For Table of Contents Use Only

Jia-wei Feng, Hong-ming Ding, Chun-lai Ren, and Yu-qiang Ma

Pumping of water by rotating chiral carbon nanotube

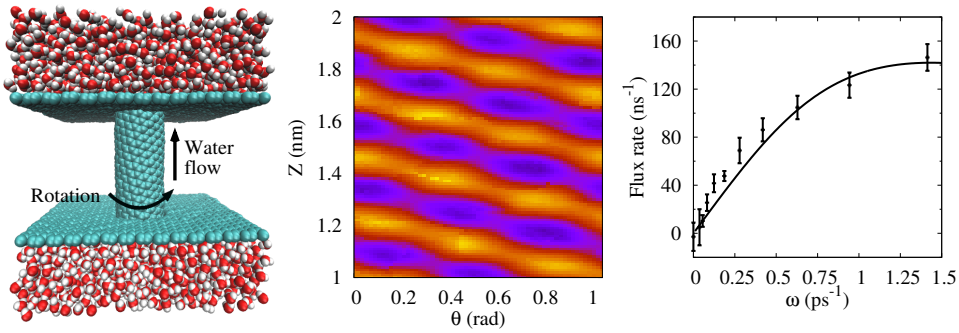

FIG. 7: By using molecular dynamics simulations, we show that the continuous pumping of water can be achieved by rotating a chiral CNT, and the simulation results are well explained by a dragging theory.